출 원 번 호 통 지 서

출 원 일 자	2021.05.21
특 기 사 항	심사청구(무) 공개신청(무) 참조번호(P210535)
출 원 번 호	10-2021-0065309 (접수번호 1-1-2021-0584912-73) (DAS접근코드6909)
출 원 인 명 칭	건국대학교 산학협력단(2-2004-015764-8)
대 리 인 성 명	김정수(9-2008-000523-0)
발 명 자 성 명	문두경 전성재 김이나 이형석 한용운
발 명 의 명 칭	유기태양전지용 dimethoxythiophene 스페이서를 도입한 유기단분자 억셉터 소재개발

특 허 청 장

<< 안내 >>

1. 귀하의 출원은 위와 같이 정상적으로 접수되었으며, 이후의 심사 진행상황은 출원번호를 이용하여 특허로 홈페이지(www.patent.go.kr)에서 확인하실 수 있습니다.
2. 출원에 따른 수수료는 접수일로부터 다음날까지 동봉된 납입영수증에 성명, 납부자번호 등을 기재하여 가까운 은행 또는 우체국에 납부하여야 합니다.
※ 납부자번호 : 0131(기관코드) + 접수번호
3. 귀하의 주소, 연락처 등의 변경사항이 있을 경우, 즉시 [특허고객번호 정보변경(경정), 정정신고서]를 제출하여야 출원 이후의 각종 통지서를 정상적으로 받을 수 있습니다.
4. 기타 심사 절차(제도)에 관한 사항은 특허청 홈페이지를 참고하시거나 특허고객상담센터(☎ 1544-8080)에 문의하여 주시기 바랍니다.
※ 심사제도 안내 : http://www.kipo.go.kr-지식재산제도

【서지사항】

【서류명】 특허출원서

【참조번호】 P210535

【출원구분】 특허출원

【출원인】

【명칭】 건국대학교 산학협력단

【특허고객번호】 2-2004-015764-8

【대리인】

【성명】 김정수

【대리인번호】 9-2008-000523-0

【포괄위임등록번호】 2016-004544-8

【발명의 국문명칭】 유기태양전지용 dimethoxythiophene 스페이서를 도입한 유기단분자 억셉터 소재개발

【발명의 영문명칭】 Dimethoxythiophene Effect as Spacer in the Molecular Design for Efficient Non-fullerene Acceptors

【발명자】

【성명】 문두경

【성명의 영문표기】 MOON, Doo Kyung

【주민등록번호】 600528-1XXXXXX

【우편번호】 06670

【주소】 서울특별시 서초구 효령로49길 57, 203동 802호(서초동, 서초2차이편한세상)

【발명자】

【성명】 전성재

【성명의 영문표기】 JEON, Sung Jae

【주민등록번호】 880529-1XXXXXX

【우편번호】 28113

【주소】 충청북도 청주시 흥덕구 옥산면 오송가락로 1056

【발명자】

【성명】 김이나

【성명의 영문표기】 KIM, Ie Na

【주민등록번호】 960315-2XXXXXX

【우편번호】 26406

【주소】 강원도 원주시 모란1길 51, 101동 704호(단계동, 단계이안 아파트)

【발명자】

【성명】 이형석

【성명의 영문표기】 LEE, Hyong Seok

【주민등록번호】 930505-1XXXXXX

【우편번호】 24547

【주소】 강원도 양구군 양구읍 중심로 77-55, 502호(서호빌라)

【발명자】

【성명】 한용운

【성명의 영문표기】 HAN, Yong Woon

【주민등록번호】 880825-1XXXXXX

【우편번호】 12966

【주소】	경기도 하남시 하남대로887번길 25, 108동 301호(덕풍동, 하남한솔솔파크)

【출원언어】 영어

【임시 명세서(청구범위제출유예)】 제출

【취지】 위와 같이 특허청장에게 제출합니다.

대리인 김정수 (서명 또는 인)

【수수료】

【출원료】	0	면	73,000	원
【가산출원료】	1	면	0	원
【우선권주장료】	0	건	0	원
【심사청구료】	0	항	0	원
【합계】	73,000 원			
【감면사유】	전담조직(50%감면)[1]			
【감면후 수수료】	36,500 원			

【임시명세서】

임시 명세서 파일 첨부(P210535_건국대_문두경_가출원명세서.PDF)

Dimethoxythiophene Effect as Spacer in the Molecular Design for Efficient Non–fullerene Acceptors

Ie Na Kim[a], Sung Jae Jeon[a], Hyong Seok Lee[a], Yong Woon Han[a], Nam Gyu Yang[a], Dong Hyeon Hong[a], Chang Ho Jung[a], and Doo Kyung Moon[a*]

[a]Nano and Information Materials (NIMs) Laboratory, Department of Chemistry Engineering, Konkuk University, 120, Neungdong–ro, Gwangjin–gu, Seoul 05029, Korea

Abstract

Three narrow bandgap non–fullerene small molecule acceptors (NFAs) – IDTT2OT, IDTT2OT–2F, and IDTT2OT–4F– were designed and synthesized using a 3,4–dimethoxythiophene as a spacer linking the indacenodithieno[3,2–*b*]thiophene (IDTT) core and 2–(3–oxo–2,2,3–dihydroinden–1–ylidene) (IC) end groups. The NFAs exhibited narrow bandgaps of 1.51, 1.45, and 1.42 eV with increased LUMO energy level of –3.69, –3.83, and –3.90 eV, respectively, owing to the extension of the conjugation length and enhanced electron push–pull environment. By finely tuning the energy level modulation effect, with a poly[2,6–4,8–bis(5–(2–ethylhexyl)thiophen–2–yl)–benzo–1,2–*b*:4,5–*b*']dithiophene])–alt(5,5–(1,3'–di–2–thienyl–5',7'–bis(2–ethylhexyl)benzo[1',2'–*c*:4',5'–*c*']dithiophene–4,8–dione)) (PBDB–T) donor, all the NFA–based devices showed the broad photo–response, at 300–900 nm, with small energy losses of 0.56–0.57 eV, and therefore enhanced the light–harvesting ability of organic solar cells. Specifically, the PBDB–T:IDTT2OT–4F device exhibited the best power conversion efficiency (10.40%) with a high J_{SC} of 19.3

mA cm^{-2} and a V_{OC} of 0.86 V. Our results demonstrate that introducing 3,4–dimethoxythiophene is an efficient strategy for improving the electron accepting ability of NFAs by tuning frontier energy levels.

Keywords : Organic solar cells, Non–fullerene small molecule acceptors, 3,4–dimethoxythiophene, Up–shifted LUMO level.

1. Introduction

With their capacity for conversion of solar light into electricity, organic solar cells (OSCs) have been studied extensively in recent decades owing to their advantages of low cost, light weight, and flexibility [1–7]. Previous studies have revealed that fullerene acceptors, although possessing strong electron mobilities and affinities, suffer from various drawbacks, including weak absorption in the visible and near–infrared (NIR) regions and a limited structural modification potential [7–11]. By contrast, non–fullerene small molecule acceptors (NFAs), containing electron withdrawing components such as benzothiadiazole, benzodithiophene, *etc*, allow simple energy level modulation and control of the absorption area through molecular design, hence NFAs development has accelerated rapidly [2,6–14]. In particular, the acceptor–donor–acceptor (A–D–A) NFAs, consisting of a fused electron–donating core and strong electron–withdrawing end groups, effectively transport charge carriers via the intramolecular push–pull effect, and their energy levels can be easily modified by varying the moieties within their structures [7–12,15–17]. Thanks to these merits, the efficiencies of OSCs have been increased by the incorporation of A–D–A NFAs, the energy levels of which can be adjusted to generate suitable offsets and enhance light–absorption matching with the donor [2,7,13].

The molecular designs of NFAs suggest various possibilities for further increases in the efficiency of NFA–based OSCs. Nowadays, narrow bandgap (<1.5 eV) NFAs, which absorb the in NIR region, are being actively investigated because of their strong light–harvesting abilities [11,12,15,16]. As NIR region accounts for

50% of the total solar radiation intensity [7], the development of narrow–bandgap NFAs is desirable for enhanced current generation and increased short–circuit current density (J_{SC}) [6,9,12,16].

For the design of A–D–A type NFAs, the introduction of π–spacer unit is a relatively straightforward method, when compared with the synthesis of fused–ring extensions to increase π–conjugation [18,19]. Via a simple synthesis sequence, an A–π–D–π–A configuration can be created to modulate the energy levels of NFAs with well–characterized central donor units. In addition, an atom with strong electronegativity in the spacer such as oxygen can be connected to other units through non–covalent interactions, facilitating planarization and intramolecular charge transfer [15,20–22]. Thus, all the effects that stem from adopting the spacer unit efficiently reduce the energy bandgap and enhance the NIR photo–response, thereby achieving higher J_{SC} for the OSC device [6].

However, there is a trade–off between the effective charge separation, which aids photocurrent generation, and voltage loss by strong non–radiative recombination in the cell [15,23]. The open–circuit voltage (V_{OC}) in an OSC device is primarily determined by the adequacy of the charge–transfer state energy [24]. When an increased J_{SC} can be obtained, a smaller offset between the lowest unoccupied molecular orbital (LUMO) level of the acceptor and the highest occupied molecular orbital (HOMO) level of the donor molecule might induce a reduction in V_{OC} [25,26]. For instance, J_{SC} enhancement achieved via broadening the NIR absorption band by decreasing the LUMO level often reduces V_{OC} [16]. Therefore, precise engineering of the frontier energy levels of active materials is required to obtain devices with desirable J_{SC} and V_{OC} values, and consequently, remarkable PCEs. To this end, up–shifting LUMO level is a good option for elevating J_{SC} without compromising on V_{OC}. In this strategy, decreased HOMO offset helps increase the gap between the acceptor LUMO and donor HOMO, thereby increasing V_{OC} and diminishing the energy loss, which is defined as the $E_{\mathrm{loss}} = E_{\mathrm{g}}^{\mathrm{opt}} - e\,V_{\mathrm{OC}}$, where $E_{\mathrm{g}}^{\mathrm{opt}}$ is the optical bandgap [11,16,27,28].

For example, Zhan et al. proved that adopting a 3,4–dimethoxythiophene spacer on NFA (IEICF–DMOT) is an efficient strategy for lifting LUMO level up comparing with an IEICO–4F acceptor which possess long branched alkoxy chain on thiophene spacer at 3–position. Up–shifted LUMO level of IEICF–DMOT effectively closed the energy offset with PBDB–T donor and exhibited higher device performance (9.98 to 13.01%), increase of V_{OC} (0.74 to 0.87 V) with slightly decreased NIR absorption (23.10 to 22.14 mA cm^{-2}) for its enlarged energy bandgap than IEICO–4F based device [21].

Moreover, Chen et al. strengthened the electron–donating ability of an acceptor by incorporating a thiophene spacer between indacenodithieno[3,2–*b*]thiophene (IDTT) core and 2–(3–oxo–2,2,3–dihydroinden–1–ylidene) (IC) end groups. ITTIC exhibited increased LUMO energy from –4.00 eV to –3.82 eV and the HOMO level from –5.55 eV to –5.28 eV, when compared with ITIC. The narrow bandgap (1.46 eV) achieved with the elevated LUMO level for ITTIC corresponded to a larger V_{OC} of 0.92 V and a broader photo–response, with a J_{SC} of 15.93 mA cm^{-2}, reduced energy loss (0.54 eV), and PCE of 9.12%, which is higher than that of the ITIC–based device [12].

Taking advantage of those strategies, we aim to raise the LUMO level and narrow its energy bandgap under 1.5 eV simultaneously through introducing a spacer, which is a suitable strategy for effective NIR absorption with minimizing voltage loss of the device. A shortest dialkoxy–functionalized thiophene spacer with planar IDTT core and IC end groups could be an effective approach to lift the LUMO energy level up and smaller the bandgap of NFAs without causing unexpected steric hindrance and altered intermolecular packing.

Herein, by introducing 3,4–dimethoxythiophene as spacer, new NFAs—IDTT2OT, IDTT2OT–2F, and IDTT2OT–4F—were designed and synthesized with the aim of precisely tuning the frontier energy level by differentially fluorine–substituted end groups. For these three acceptors, small E_g^{opt} values of 1.51, 1.45, and 1.42 eV are obtained with increased LUMO energy levels of –3.69, –3.83, and –3.90 eV, respectively, which are relatively high–lying LUMO levels than those of other NIR bandgap acceptors [15,21,29,30]. Further photovoltaic optimization revealed that IDTT2OT–4F based OSCs exhibited the best PCE of 10.40%, a reasonably high J_{SC} of 19.3 mA cm^{-2}, V_{OC} of 0.86 V, and a fill factor (FF) of 62.4% owing to the strong photo–response at 300–900 nm, with small E_{loss} of 0.56 eV.

2. Experimental section

2.1 Theoretical simulation

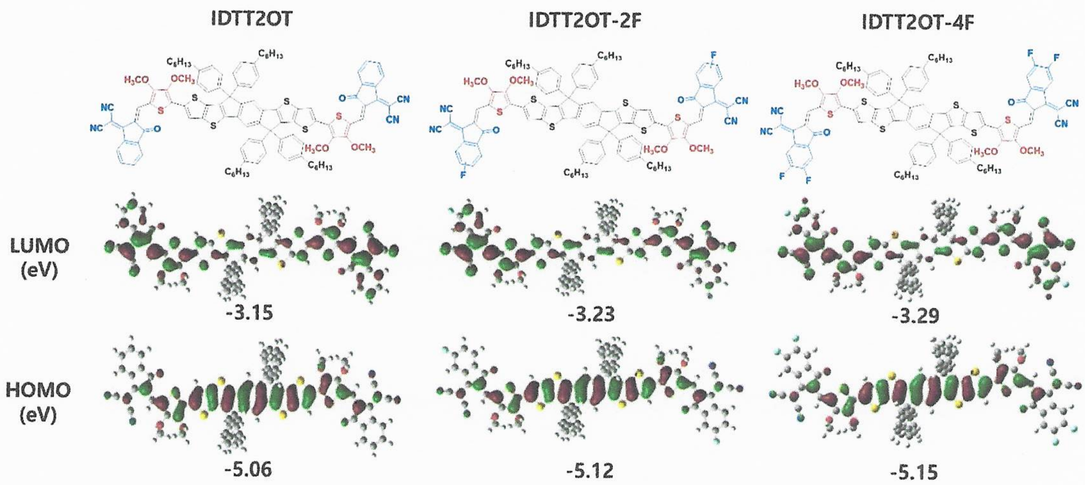

Figure 1. Chemical structure and theoretical calculation of IDTT2OT, IDTT2OT–2F, and IDTT2OT–4F

Initially, density functional theory (DFT) calculations were carried out to evaluate the optimized energy levels and geometries of IDTT2OT, IDTT2OT–2F, and IDTT2OT–4F. ITTIC, which has no methoxy chains on the thiophene spacer, as reported by Chen et al., was also examined to better understand the electronic system (**Figure S1**). For all NFAs, the HOMO energy mainly spread along the conjugated core, and the LUMO energy delocalized over the entire molecules, especially on the end groups (**Figure 1**). Compared with ITTIC, IDTT2OT shows higher LUMO and HOMO by 0.12 and 0.14 eV, respectively, meaning the introduction of a dimethoxy chain is an effective strategy for narrowing the energy bandgap by raising the LUMO level of NFAs, which would result in enhanced V_{OC} in devices. As fluorination can occur at the two edges of an IC unit, the energy levels of the three isomers of IDTT2OT–2F, shown in **Figure S2**, have the same HOMO but slightly different LUMO levels. IDTT2OT–4F exhibits the lowest frontier energy levels among the NFAs (**Figure 1**), coincident with the effect of fluorination on the NFAs, which is expected to lower the frontier energy levels and increase photon absorption in the longer wavelength region by narrowing the bandgap [31]. Furthermore, all three NFAs exhibit a small dihedral angle of ~0.38° between the flat IDTT core and spacer and ~3.28° between the end group and spacer (**Figure S3**). With non–covalent interactions among the units as well as small dihedral angles and planar backbone, the strong intramolecular interactions and flat conformation of could be ascribed to an effective charge separation [14,32,33]. Owing to the maintenance of the planar backbone, the three NFAs exhibit near–zero dipole moments (**Table S1**).

2.2 Materials synthesis

Unless otherwise noted, all chemicals used in the syntheses were purchased from Aldrich, Alfa Aesar, Acros, or TCI, and used without further purification; (4,4,9,9,–tetrakis(*p*–hexylphenyl)–4,9–dihydro–s–indaceno[1,2–*b*:5,6–*b*']dithiophene–2,8–diyl)bis(trimethylstannane) (IDTT–$SnMe_3$) was purchased from Sunatech Inc. All reactions were performed under nitrogen atmosphere and checked by thin layer chromatography (TLC) on silica gel. Column chromatography was conducted using silica gel 60 (230–400 mesh ASTM, Merck).

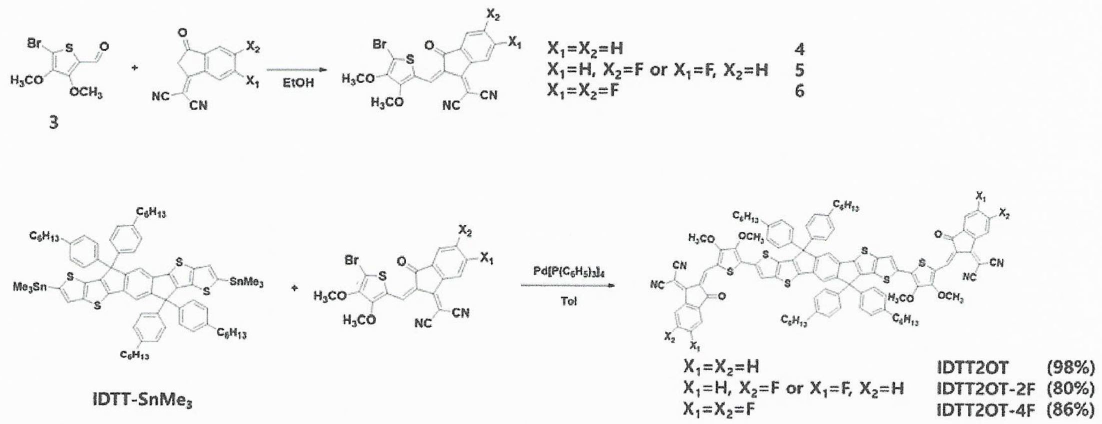

Scheme 1. Synthetic route for IDTT2OT, IDTT2OT–2F, and IDTT2OT–4F

IDTT2OT, IDTT2OT–2F, and IDTT2OT–4F were synthesized through **Scheme 1**; the synthesis details are given in the supporting information. With nucleophilic substitution of 3,4–dibromothiophene, 3,4–dimethoxythiophene (**1**) was synthesized with a yield of 61%; 3,4–dimethoxythiophene–2–carbaldehyde (**2**) was synthesized through the Vilsmeire–Haack reaction with a yield of 67% and brominated with a yield of 75%. Through Knoevenagel condensation with (**3**) and IC, IC–F, and IC–2F, the products OT–IC (**4**), OT–IC–F (**5**), and OT–IC–2F (**6**), respectively, were synthesized and used without purification. Finally, IDTT2OT (**7**), IDTT2OT–2F (**8**), and IDTT2OT–4F (**9**) were synthesized through Stille coupling reaction between IDTT–$SnMe_3$ and (**4**), (**5**), and (**6**), with the palladium catalyst under toluene, with a yield of 98%, 80%, and 86%, respectively. The chemical structure of the intermediate materials was characterized using ^{1}H NMR, and IDTT2OT, IDTT2OT–2F, and IDTT2OT–4F were fully characterized through ^{1}H NMR, ^{13}C NMR **(Figure S4–S12),** and MALDI–TOF. IDTT2OT, IDTT2OT–2F, and IDTT2OT–4F are soluble in common solvents such as chloroform ($CHCl_3$), tetrahydrofuran (THF), chlorobenzene (CB) at room temperature.

3. Results and discussion

3.1 Thermal Properties

The thermal properties of the three NFAs were investigated by thermogravimetric analysis (TGA) and differential scanning calorimetry (DSC) (**Figure S13**). The NFAs exhibited good thermal stability with decomposition temperatures (5% weight loss) of 343, 353, and 344 °C for IDTT2OT, IDTT2OT–2F, and IDTT2OT–4F, respectively, which is adequate for photovoltaic devices. The DSC curves of IDTT2OT and IDTT2OT–2F showed exothermic peaks during the first heating scan, when partial rearrangement occurred and crystalline states were generated [34–36]. IDTT2OT displays a cold crystallization peak at ~229 °C, whereas IDTT2OT–2F has peaks at ~230 °C and ~256 °C, indicating its enhanced crystallinity among the NFAs. By contrast, IDTT2OT–4F has no peak in the heating range, suggesting that it possesses the most amorphous nature among the NFAs [37].

3.2 Optical and Electrochemical properties

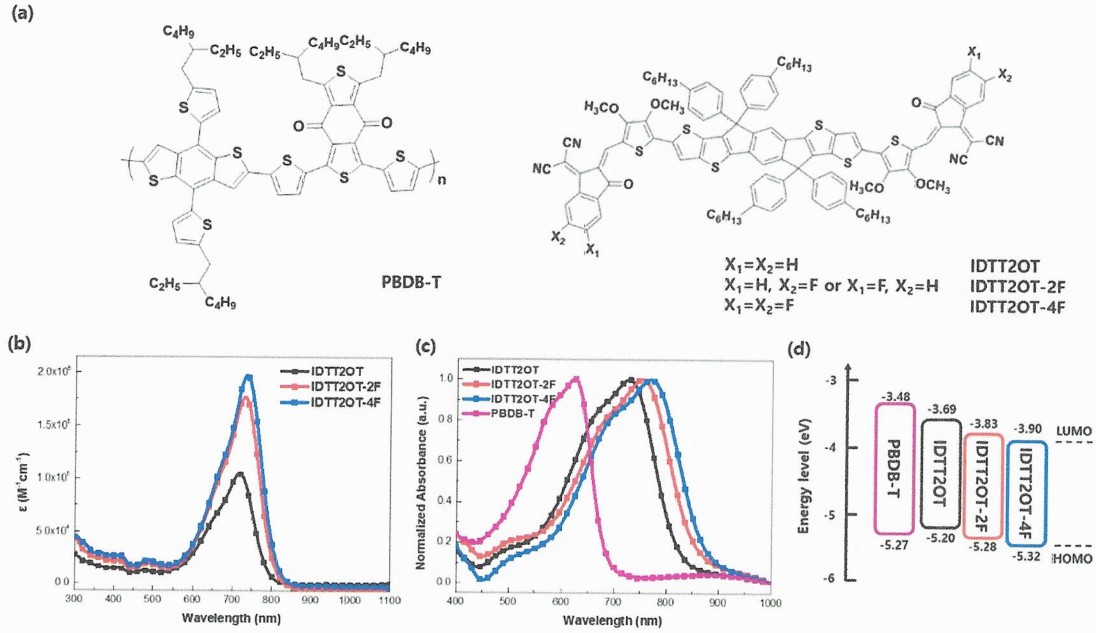

Figure 2. (a) Molecular structures, (b) molar absorption coefficients in dilute chloroform solution, (c) UV–vis absorption spectra on thin films, and (d) energy level diagrams of PBDB–T, IDTT2OT, IDTT2OT–2F, and IDTT2OT–4F

The absorption spectra of the NFAs in chloroform and as films are shown in **Figure 2b and c** and listed in **Table 1.** With four different dilute chloroform solutions, the molar absorption coefficient of the NFAs is calculated using the Beer–Lambert equation: $A = \varepsilon bc$, where A is the absorbance, ε is the molar absorption coefficient, b is the length of the light path, and c is the concentration of acceptors in the solution. The average values of the molar absorption coefficient of the NFAs are measured to be 1.09×10^{-5}, 1.77×10^{-5}, and 2.03×10^{-5} M^{-1} cm^{-1} at the $\lambda_{max,sol}$ values of 717, 731, and 734 nm, respectively. With their high molar absorption coefficient values at the maximized wavelength, all NFAs are expected to have effective photon harvesting ability [14]. Thin films of the NFAs exhibit broader and red–shifted absorption than those in solution; the absorption edges of the NFAs are located at 820, 856, and 873 nm, corresponding to the narrow optical bandgaps of 1.51, 1.45, and 1.42 eV, respectively.

The electrochemical properties of NFAs were investigated by cyclic voltammetry (CV) (**Figure S14**).

From the measured onset oxidation potential $E_{\mathrm{onset}}^{\mathrm{ox}}$ values, the HOMO energies of IDTT2OT, IDTT2OT–2F, and IDTT2OT–4F were calculated to be –5.20, –5.28, and –5.32 eV and the LUMO energies to be –3.69, –3.83, and –3.90 eV, respectively (**Table 1**). As co–facial stacking between the molecules increases with the number of fluorine atoms, the frontier energy levels of the NFAs are lowered and the bandgaps narrowed [6].

Table 1. Optical and electrochemical properties of IDTT2OT, IDTT2OT–2F, and IDTT2OT–4F

NFAs	UV–vis absorption					CV	
	$\lambda_{\mathrm{max,sol}}$ [nm]	$\lambda_{\mathrm{max,film}}$ [nm]	λ_{onset} [nm]	$E_{\mathrm{g}}^{\mathrm{opt}}$ a) [eV]	ε [$M^{-1}cm^{-1}$]	E_{HOMO} b) [eV]	E_{LUMO} c) [eV]
IDTT2OT	717	725	820	1.51	1.09×10^{-5}	–5.20	–3.69
IDTT2OT–2F	731	754	856	1.45	1.77×10^{-5}	–5.28	–3.83
IDTT2OT–4F	734	768	873	1.42	2.03×10^{-5}	–5.32	–3.90

a) $E_{\mathrm{g}}^{\mathrm{opt}} = 1240/\lambda_{\mathrm{onset}}$, b) $E_{\mathrm{HOMO}} = -\left(E_{\mathrm{onset}}^{\mathrm{ox}} - E_{\frac{1}{2},\mathrm{ferrocene}}\right) - 4.8\ eV$, c) $E_{\mathrm{LUMO}} = E_{\mathrm{HOMO}} - E_{\mathrm{g}}^{\mathrm{opt}}$

Poly[2,6–4,8–bis(5–(2–ethylhexyl)thiophen–2–yl)–benzo–1,2–b:4,5–*b*1']dithiophene])–alt(5,5–(1,3'–di–2–thienyl–5',7'–bis(2– ethylhexyl)benzo[1',2'–*c*:4',5'–*c*']dithiophene–4,8–dione)) (PBDB–T) was selected as donor owing to its strong absorption in the 500–700 nm range, which complements the NFAs' absorption (**Figure S15b**). The HOMO and LUMO energy levels of PBDB–T were calculated to be –5.27 eV and –3.48 eV, respectively. IDTT2OT–2F and IDTT2OT–4F display well–matched energy level alignments, whereas a small negative HOMO offset exists for IDTT2OT, which may not be beneficial for hole transfer between donor and acceptor [23].

3.3 Photovoltaic properties

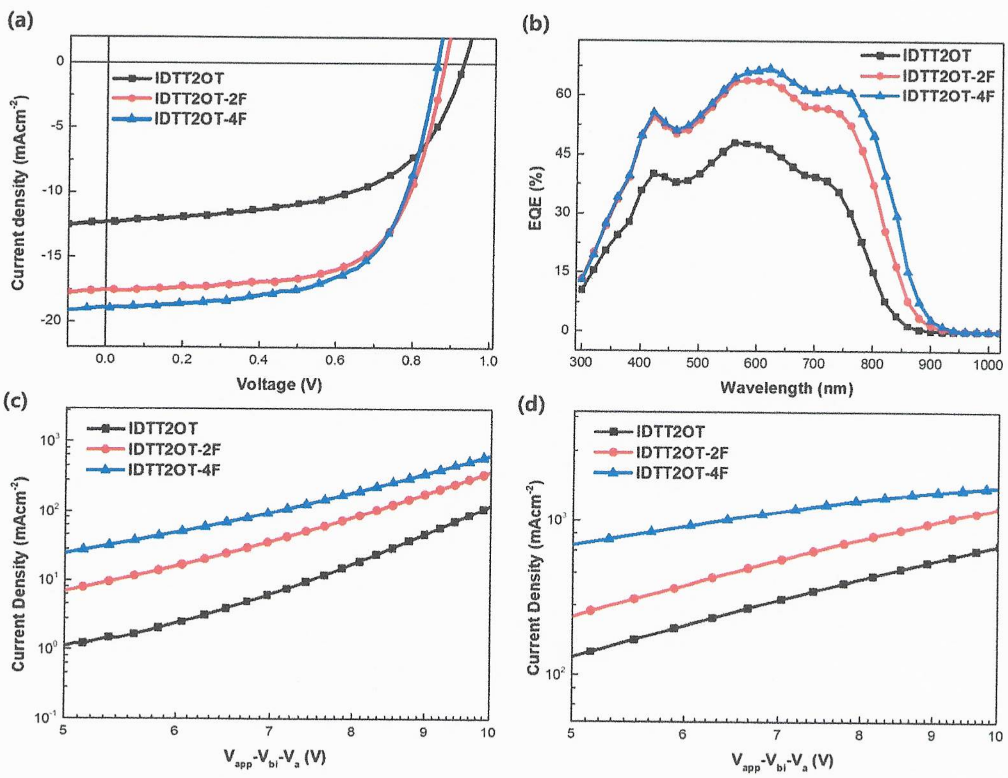

Figure 3. (a) J–V curves, (b) EQE spectra, (c) electron mobility, and (d) hole mobility as obtained using SCLC methods.

Inverted–structured OSCs were fabricated with ITO/ZnO/PBDB–T:NFAs/MoO_3/Ag architecture. The devices were optimized by thermal annealing at 100 °C for 10 min and high–boiling point solvent additives such as 1,8–diodoocatane (DIO), 1–chloroaphthalene (CN), and diphenyl ether (DPE) were used for enhancing the miscibility through the formation of a bicontinous interpenetrating network [38]. The *J–V* curves of the best performing NFA–based devices are displayed in **Figure 3a** and their photovoltaic parameters are listed in **Table 2**. The IDTT2OT–4F devices exhibited J_{SC} of 19.3 mA cm^{-2}, V_{OC} of 0.86 V, FF of 62.4%, and PCE of 10.40%; these values represented the best performance among the NFA devices. In the case of the IDTT2OT device, a moderate PCE was obtained, although the device exhibited a negative

HOMO offset with the donor and thereby insufficient driving force for charge transfer. With more fluorine substitution, the reduced energy bandgaps of IDTT2OT–2F and IDTT2OT–4F resulted in enhanced photo–responses, whereas the greater gap between donor HOMO and acceptor LUMO caused V_{OC} to drop. Nevertheless, the IDTT2OT–4F device showed the most extended photon absorption, with a PCE of 10.40%, among the NFAs. With the high–lying LUMO energy level strategy, the small E_{loss} of 0.56 eV for the IDTT2OT–4F device compensates its decrease in V_{OC}, thereby providing an overall PCE boost for the OSCs via enhanced photon absorption [5,30].

Table 2. Photovoltaic parameters of IDTT2OT, IDTT2OT–2F, and IDTT2OT–4F based devices

PBDB–T:NFAs	V_{OC} [V]	J_{SC} [mA cm^{-2}]	J_{SC}^{cal} [mA cm^{-2}]	FF [%]	PCE$_{max}$ (PCE$_{ave}$$^{a)}$) [%]	E_{loss} [V]
IDTT2OT	0.95	11.4	10.9	59.7	6.43 (6.36 ± 0.07)	0.56
IDTT2OT–2F	0.88	17.5	16.1	65.1	10.04 (9.79 ± 0.25)	0.57
IDTT2OT–4F	0.86	19.3	18.7	62.4	10.40 (10.18 ± 0.22)	0.56

[a]) Average values with standard deviation from over eight devices

External quantum efficiency (EQE) measurements were conducted for the optimized devices built using each of the acceptors and PBDB–T, and the corresponding curves are presented in **Figure 3b** and **Table 2.** For the three devices, the entire EQE response occurs between 300 nm and 900 nm, signifying that the PBDB–T polymer donor and all three NFAs simultaneously contribute to the J_{SC} values, in agreement with the *J–V* characteristics. Specifically, as the IDTT2OT–4F has the most extended absorption in the NIR region, the highest EQE response was obtained for the PBDB–T:IDTT2OT–4F device.

3.4 Charge transfer and mobilities

Charge transfer and photo–induced exciton dissociation were monitored using photoluminescence (PL) spectroscopy. Spectra of the pristine PBDB–T, IDTT2OT, IDTT2OT–2F, and IDTT2OT–4F and optimized blended films were measured, with excitation at 550 nm and 650 nm, as shown in **Figure S16**. The PL quenching efficiencies of the PBDB–T:IDTT2OT, PBDB–T:IDTT2OT–2F, and PBDB–T:IDTT2OT–4F films were measured to be 65%, 67%, and 68%, respectively, at 550 nm and 68%, 73%, and 80%, respectively, at 650 nm. As the increased quenching in the blends promotes photo–induced charge transfer, the IDTT2OT–4F blend film exhibits most effective electron transfer from donor to acceptor, which is consistent with its best photovoltaic performance [39]. Interestingly, the IDTT2OT blend film exhibited a quenching rate comparable with the other blend films at both excitation wavelengths, although the blend has a negative HOMO offset, which could result in slower hole transfer and lower efficiency [28,40].

Table 3. Electron and hole mobilities of the IDTT2OT, IDTT2OT–2F, and IDTT2OT–4F based films

	μ_e [$cm^2 V^{-1} s^{-1}$]	μ_h [$cm^2 V^{-1} s^{-1}$]	μ_e/μ_h
IDTT2OT	9.22×10^{-5}	3.02×10^{-4}	0.305
IDTT2OT–2F	5.67×10^{-4}	6.62×10^{-4}	0.856
IDTT2OT–4F	7.94×10^{-4}	8.52×10^{-4}	0.932

The space–charge–limited current (SCLC) method was adopted (**Figure 3c and d**) and the charge mobilities were determined by fitting the dark current according to the modified Mott–Gurney equation [14,20]. In the $J = 9\varepsilon_r\varepsilon_0\mu_{eff}V^2/8L^3$, J is the dark current density (mA cm^{-2}), ε_r is the permittivity of free space (8.85×10^{-12} F cm^{-1}), ε_0 is the dielectric constant of the blend material (assumed to be 3.0), μ_{eff} is the carrier mobility, V is the effective voltage, and L is the thickness of the active layer (120 nm).

The electron only devices with ITO/ZnO/PBDB–T:NFAs/PDINO/Ag structures and hole–only devices with ITO/PEDOT:PSS/PBDB–T:NFAs/PEDOT:PSS/Ag structures were fabricated, and each of the observed mobilities is listed in **Table 3**. The PBDB–T:IDTT2OT–4F device possessed the most balanced

μ_e/μ_h value of 0.93 with highest electron mobility of 7.94 × 10^{-4} cm^2 V^{-1} s^{-1} and hole mobility of 8.52 × 10^{-4} cm^2 V^{-1} s^{-1}, which indicates enhanced structural order for the blend and better charge extraction [16]. Moreover, with its negative HOMO offset, the PBDB–T:IDTT2OT device has imbalanced mobilities, which hampers further J_{SC} improvement [41]. The PL quenching and SCLC results demonstrate the validity of introducing 3,4-dimethoxythiophene, an effective strategy for charge separation in the device, although the energy level impedes effective charge transfer.

3.5 Structural order and morphology

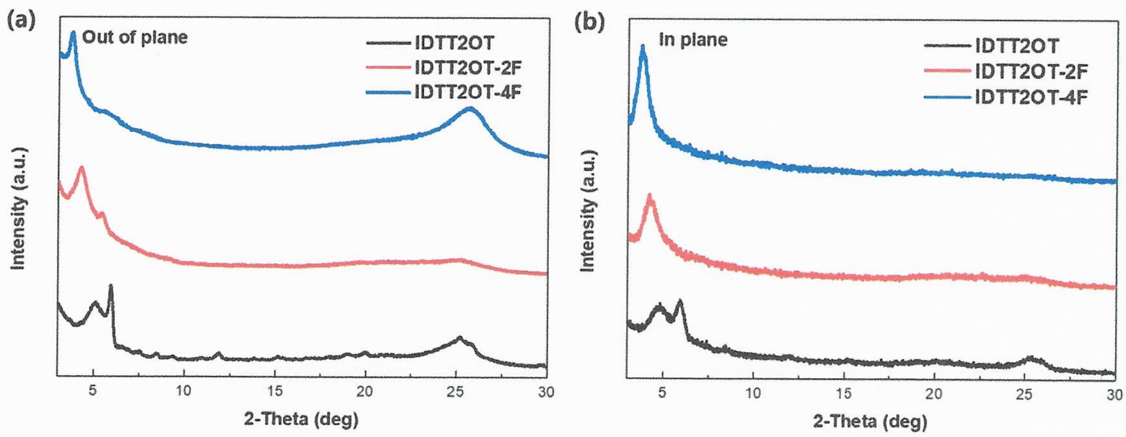

Figure 4. XRD images of IDTT2OT, IDTT2OT–2F, and IDTT2OT–4F acquired with (a) out–of–plane and (b) in–plane irradiation.

As nanostructured ordering effects, from exciton diffusion to charge collection, are correlated with the performance of the device [35], solid state of the pristine NFAs film were studied by X–ray diffraction (XRD). This method allowed identification of the crystalline texture through the diffraction peak structure (**Figure 4**). From the out–of–plane (OOP) irradiation measurement, (100) lamellar d–spacings (d_l) of 17.36, 20.67, and 23.60 Å were obtained for the pure–NFA films. The (010) π–π stacking diffraction peak, with distances of 3.51, 3.54, and 3.46 Å, respectively, indicates face–to–face stacking behavior [32]. The shortest π–π stacking distance of IDTT2OT–4F indicates that the introduction of fluorine atoms to the molecular backbone enables the formation of compact packing via stronger interchain networks [13,42]. Moreover, the intense (010) peak in the spectrum of the IDTT2OT–4F film, which becomes faint in the in–plane (IP) direction, demonstrates the predominant face–on orientation [15,31]. With the preferential face–on orientation and the short π–π stacking distance, the IDTT2OT–4F film exhibits superior charge transport and exciton extraction, which contribute to the elevated J_{SC} when it is incorporated into photovoltaic devices [30]. Intense (100), (001) backbone, and (010) diffraction peaks are observed in both the OOP and IP directions for the pristine IDTT2OT film, suggesting bimodal edge–on and face–on crystallites [14,31]. The observable (100) and (001) peaks in the OOP and IP spectra and faint (010) peak in the OOP spectrum, which does not appear in the IP spectrum, suggest that IDTT2OT–2F exhibits crystallinity, but with quiet disordered orientation and a relatively large stacking distance for the existence of isomers.

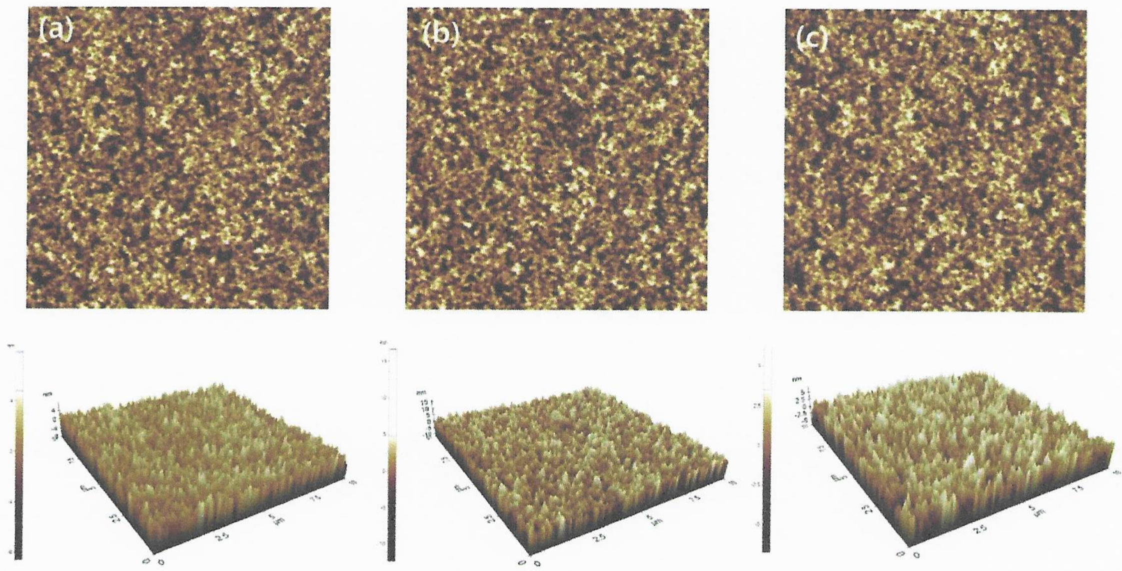

Figure 5. 2D and 3D AFM topographies (10 μm × 10 μm) of (a) PBDB–T:IDTT2OT, (b) PBDB–T:IDTT2OT–2F, and (c) PBDB–T:IDTT2OT–4F.

The morphologies of the PBDB–T:NFAs thin films were analyzed by atomic force microscopy (AFM) (**Figure 5**). Light and dark areas in the AFM images indicate aggregation of the polymer and acceptors, respectively [16,32]. All the blended films exhibited smooth surface features, with comparable root–mean–square (RMS) roughness values of 1.75, 2.12, and 1.69 nm, for the PBDB–T:IDTT2OT, PBDB–T:IDTT2OT–2F, and PBDB–T:IDTT2OT–4F films, respectively, which implies interpenetrating networks were generated in all the blended films. Larger RMS roughness values correspond to reduced charge–carrier transport [25]; hence, the IDTT2OT–4F blended film exhibited the lowest RMS roughness. Its fibrous surface forms an efficient interface, which is beneficial for exciton generation and charge transfer, and thus results in the enhancement of the device characteristics.

4. Conclusion

In summary, IDTT2OT, IDTT2OT–2F, and IDTT2OT–4F, introducing the 3,4–dimethoxythiophene spacer between the planar IDTT core and IC groups, were designed to narrow the energy bandgap and increase the LUMO energy level with enlarged electron–donating ability. Through moderate fluorination within the end groups of the acceptors, enhanced absorption spectra in the NIR region were observed for the NFAs, thereby enhancing the photo–response of solar cell devices. With the best results in terms of the photocurrent and V_{OC}, the IDTT2OT–4F based device exhibits the photovoltaic performance of 10.40% with J_{SC} of 19.3 mA cm^{-2}, V_{OC} of 0.86 V, and FF of 62.4%, which indicates the highest PCE among the three NFAs. With its preferential face–on orientation, IDTT2OT–4F exhibits good mixing with the crystalline PBDB–T donor polymer, yielding the highest and most balanced charge transfer and mobility. Our results demonstrate that selecting the 3,4–dimethoxythiophene units and enhancing the electron–donating properties of the acceptors, by enlarging the NIR absorption band and increasing the LUMO energy level, is an efficient energy level modulation strategy in NFAs for improving the photovoltaic performance of NFA–based OSCs.

Author Information

Corresponding Authors

*Tel.: +82–2–450–3498, Fax: +82–2–444–0765

*E–mail: dkmoon@konkuk.ac.kr

Acknowledgments

This paper was supported by Konkuk University in 2019.This research was supported by the Korea Institute of Energy Technology Evaluation and Planning (KETEP) and the Ministry of Trade, Industry & Energy (MOTIE) of the Republic of Korea (No. 20193091010110), the National Research Foundation of Koea (NRF) grant funded by the Korea government (MSIT) (No. 2020R1A2C201091611), and the Human Resources Program (no. 20194010201790) of the Korea Institute of Energy Technology Evaluation and Planning (KETEP).

Reference

[1] Yu G, Gao J, Hummelen JC, Wudl F, Heeger AJ. device structure consisted Polymer Photovoltaic Cells : Enhanced Efficiencies via a Network of Internal Donor–Acceptor Heterojunctions. Science 1995;270:1789–91. https://doi.org/10.1126/science.270.5243.1789.

[2] Bauer N, Zhang Q, Zhao J, Ye L, Kim JH, Constantinou I, et al. Comparing non–fullerene acceptors with fullerene in polymer solar cells: a case study with FTAZ and PyCNTAZ. J Mater Chem A 2017;5:4886–93. https://doi.org/10.1039/c6ta10450a.

[3] Zheng B, Huo L, Li Y. Benzodithiophenedione–based polymers: recent advances in organic photovoltaics. NPG Asia Mater 2020;12:1–22. https://doi.org/10.1038/s41427–019–0163–5.

[4]. Yuan J, Zhang Y, Zhou L, Zhang G, Yip HL, Lau TK, et al. Single–Junction Organic Solar Cell with over 15% Efficiency Using Fused–Ring Acceptor with Electron–Deficient Core. Joule 2019;3:1140–51. https://doi.org/10.1016/j.joule.2019.01.004.

[5] Ma Y, Zhang M, Tang Y, Ma W, Zheng Q. Angular–Shaped Dithienonaphthalene–Based Nonfullerene Acceptor for High–Performance Polymer Solar Cells with Large Open–Circuit Voltages and Minimal Energy Losses. Chem Mater 2017;29:9775–85. https://doi.org/10.1021/acs.chemmater.7b03770.

[6] Wang Z, Huang K, Chen X, Xu Y, Xu Z, He T, et al. A high–performance non–fullerene electron acceptor with bisalkylthiothiophene π–bridges for organic photovoltaics. J Mater Chem C 2019;7:14499–503. https://doi.org/10.1039/c9tc05166j

[7] Cheng P, Li G, Zhan X, Yang Y. Next–generation organic photovoltaics based on non–fullerene acceptors /639/301/299/946 /639/624/399 review–article. Nat Photonics 2018;12:131–42. https://doi.org/10.1038/s41566–018–0104–9.

[8]. Lin Y, Zhang ZG, Bai H, Wang J, Yao Y, Li Y, et al. High–performance fullerene–free polymer solar cells with 6.31% efficiency. Energy Environ Sci 2015;8:610–6. . https://doi.org/10.1039/c4ee03424d.

[9] Lee TH, Kim DH, Lee EJ, Moon DK. Significant impact of monomer curvatures for polymer curved shape composition on backbone orientation and solar cell performances. J Ind Eng Chem 2018;65:195–204. https://doi.org/10.1016/j.jiec.2018.04.029.

[10] Liu Y, Zhang C, Hao D, Zhang Z, Wu L, Li M, et al. Enhancing the Performance of Organic Solar Cells by Hierarchically Supramolecular Self–Assembly of Fused–Ring Electron Acceptors. Chem Mater 2018;30:4307–12. https://doi.org/10.1021/acs.chemmater.8b01319.

[11]. Yin P, Wang L, Liang J, Yu Y, Chen L, Weng C, et al. A small–molecule/fullerene acceptor alloy: A powerful tool to enhance the device efficiency and thermal stability of ternary polymer solar cells. J Mater Chem C 2020;8:11223–38. https://doi.org/10.1039/d0tc00329h.

[12] Liu D, Wang T, Ke X, Zheng N, Chang Z, Xie Z, et al. Ultra–narrow bandgap non–fullerene acceptors for organic solar cells with low energy loss. Mater Chem Front 2019;3:2157–63. https://doi.org/10.1039/c9qm00505f.

[13] Su D, Li K, Liu W, Zhang W, Li X, Wu Y, et al. High–Performance Ternary Polymer Solar Cells Enabled by a New Narrow Bandgap Nonfullerene Small Molecule Acceptor with a Higher LUMO Level. Macromol Rapid Commun 2020;41:1–10. https://doi.org/10.1002/marc.202000393.

[14] Yu JE, Jeon SJ, Choi JY, Han YW, Ko EJ, Moon DK. A 3–Fluoro–4–hexylthiophene–Based Wide Bandgap Donor Polymer for 10.9% Efficiency Eco–Friendly Nonfullerene Organic Solar Cells. Small 2019;15:1–10. https://doi.org/10.1002/smll.201805321.

[15] Zhang Z, Liu W, Rehman T, Ju HX, Mai J, Lu X, et al. Energy–level modulation of non–fullerene acceptors to achieve high–efficiency polymer solar cells at a diminished energy offset. J Mater Chem A 2017;5:9649–54. . https://doi.org/10.1039/c7ta01554b.

[16]. Lee J, Ko SJ, Seifrid M, Lee H, Luginbuhl BR, Karki A, et al. Bandgap Narrowing in Non–Fullerene Acceptors: Single Atom Substitution Leads to High Optoelectronic Response Beyond 1000 nm. Adv Energy Mater 2018;8:1–6. https://doi.org/10.1002/aenm.201801212.

[17]. Shi X, Chen J, Gao K, Zuo L, Yao Z, Liu F, et al. Terthieno[3,2–b]Thiophene (6T) Based Low Bandgap Fused–Ring Electron Acceptor for Highly Efficient Solar Cells with a High Short–Circuit Current Density and Low Open–Circuit Voltage Loss. Adv Energy Mater 2018;8:2–9. https://doi.org/10.1002/aenm.201702831.

[18] Cui Y, Yao H, Zhang J, Xian K, Zhang T, Hong L, et al. Single–Junction Organic Photovoltaic Cells with Approaching 18% Efficiency. Adv Mater 2020;32:1–7. https://doi.org/10.1002/adma.201908205.

[19] Ko SJ, Hoang QV, Song CE, Uddin MA, Lim E, Park SY, et al. High–efficiency photovoltaic cells with wide optical band gap polymers based on fluorinated phenylene–alkoxybenzothiadiazole. Energy Environ Sci 2017;10:1443–55. https://doi.org/10.1039/c6ee03051c.

[20] Han YW, Song HJ, Jeon SJ, Lee HS, Ko EJ, Song CE, et al. Excellent carrier transport materials produced by controlled molecular stacking and their application in flexible organic electronic devices. J Mater Chem A 2019;7:14790–805. https://doi.org/10.1039/c9ta02213a.

[21] Chang Y, Zhang X, Tang Y, Gupta M, Su D, Liang J, et al. 14%–Efficiency Fullerene–Free Ternary Solar Cell Enabled By Designing a Short Side–Chain Substituted Small–Molecule Acceptor. Nano Energy 2019;64:103934. https://doi.org/10.1016/j.nanoen.2019.103934.

[22] Jiang P, Ming S, Jia QQ, Liu Y, Lu H, Li M, et al. The influence of the π–bridging unit of fused–ring acceptors on the performance of organic solar cells. J Mater Chem A 2018;6:21335–40.

https://doi.org/10.1039/c8ta08410f.

[23] Cnops K, Zango G, Genoe J, Heremans P, Martinez–Diaz MV, Torres T, et al. Energy Level Tuning of Non–Fullerene Acceptors in Organic Solar Cells. J Am Chem Soc 2015;137:8991–7. https://doi.org/10.1021/jacs.5b02808

[24] Ghasemi M, Hu H, Peng Z, Rech JJ, Angunawela I, Carpenter JH, et al. Delineation of Thermodynamic and Kinetic Factors that Control Stability in Non–fullerene Organic Solar Cells. Joule 2019;3:1328–48. https://doi.org/10.1016/j.joule.2019.03.020.

[25] Graham KR, Erwin P, Nordlund D, Vandewal K, Li R, Ngongang Ndjawa GO, et al. Re–evaluating the role of sterics and electronic coupling in determining the open–circuit voltage of organic solar cells. Adv Mater 2013;25:6076–82. https://doi.org/10.1002/adma.201301319.

[26]. Li S, Ye L, Zhao W, Zhang S, Mukherjee S, Ade H, et al. Energy–Level Modulation of Small–Molecule Electron Acceptors to Achieve over 12% Efficiency in Polymer Solar Cells. Adv Mater 2016;28:9423–9. https://doi.org/10.1002/adma.201602776.

[27] Kini GP, Choi JY, Jeon SJ, Suh IS, Moon DK. Controlling the interchain packing and photovoltaic properties via fluorine substitution in terpolymers based on benzo[1,2–c:4,5–c']dithiophene–4,8–dione and benzothiadiazole units. Polymer (Guildf) 2018;148:330–8. https://doi.org/10.1016/j.polymer.2018.06.038.

[28] Zhang Z, Wang H, Yu J, Sun R, Xu J, Yang L, et al. Modification on the Indacenodithieno[3,2– b]thiophene Core to Achieve Higher Current and Reduced Energy Loss for Nonfullerene Solar Cells . Chem Mater 2020;32:1297–307. https://doi.org/10.1021/acs.chemmater.9b04911.

[29] Lee TH, Park SY, Walker B, Ko SJ, Heo J, Woo HY, et al. A universal processing additive for high–performance polymer solar cells. RSC Adv 2017;7:7476–82. https://doi.org/10.1039/c6ra27944a.

[30] Li X, Yan T, Bin H, Han G, Xue L, Liu F, et al. Insertion of double bond π–bridges of A–D–A acceptors for high performance near–infrared polymer solar cells. J Mater Chem A 2017;5:22588–97. https://doi.org/10.1039/c7ta07049g

[31] Li C, Yue Q, Wu H, Li B, Fan H, Zhu X. Small bandgap non–fullerene acceptor enables efficient PTB7–Th

solar cell with near 0 eV HOMO offset. J Energy Chem 2021;52:60–6. https://doi.org/10.1016/j.jechem.2020.03.058.

[32] Liao Q, Wang Y, Uddin MA, Chen J, Guo H, Shi S, et al. Drastic Effects of Fluorination on Backbone Conformation of Head–to–Head Bithiophene–Based Polymer Semiconductors. ACS Macro Lett 2018;7:519–24. https://doi.org/10.1021/acsmacrolett.8b00032.

[33] Nam SJ, Jeon SJ, Han YW, Moon DK. Effect of non–covalent interactions on molecular stacking and photovoltaic properties in organic photovoltaics. J Ind Eng Chem 2018;63:191–200. https://doi.org/10.1016/j.jiec.2018.02.015.

[34] Lin Y, Wang J, Zhang ZG, Bai H, Li Y, Zhu D, et al. An electron acceptor challenging fullerenes for efficient polymer solar cells. Adv Mater 2015;27:1170–4. https://doi.org/10.1002/adma.201404317.

[35] Bin H, Zhang ZG, Gao L, Chen S, Zhong L, Xue L, et al. Non–Fullerene Polymer Solar Cells Based on Alkylthio and Fluorine Substituted 2D–Conjugated Polymers Reach 9.5% Efficiency. J Am Chem Soc 2016;138:4657–64. https://doi.org/10.1021/jacs.6b01744.

[36] Zhang Z, Miao J, Ding Z, Kan B, Lin B, Wan X, et al. Efficient and thermally stable organic solar cells based on small molecule donor and polymer acceptor. Nat Commun 2019;10:1–8. https://doi.org/10.1038/s41467–019–10984–6.

[37] Zhang H, Li S, Xu B, Yao H, Yang B, Hou J. Fullerene–free polymer solar cell based on a polythiophene derivative with an unprecedented energy loss of less than 0.5 eV. J Mater Chem A 2016;4:18043–9. https://doi.org/10.1039/c6ta07672f.

[38] Chen M, Liu D, Li W, Gurney RS, Li D, Cai J, et al. Influences of Non–fullerene Acceptor Fluorination on Three–Dimensional Morphology and Photovoltaic Properties of Organic Solar Cells. ACS Appl Mater Interfaces 2019;11:26194–203. https://doi.org/10.1021/acsami.9b07317.

[39] Xin J, Meng X, Xu X, Zhu Q, Naveed HB, Ma W. Cold Crystallization Temperature Correlated Phase Separation, Performance, and Stability of Polymer Solar Cells. Matter 2019;1:1316–30. https://doi.org/10.1016/j.matt.2019.06.011.

[40] Li S, Zhan L, Sun C, Zhu H, Zhou G, Yang W, et al. Highly Efficient Fullerene–Free Organic Solar Cells Operate at Near Zero Highest Occupied Molecular Orbital Offsets. J Am Chem Soc 2019;141:3073–82. https://doi.org/10.1021/jacs.8b12126.

[41] Bin H, Yang Y, Peng Z, Ye L, Yao J, Zhong L, et al. Effect of Alkylsilyl Side–Chain Structure on Photovoltaic Properties of Conjugated Polymer Donors. Adv Energy Mater 2018;8:1–8. https://doi.org/10.1002/aenm.201702324.

[42] Jeon SJ, Han YW, Moon DK. Drastic Changes in Properties of Donor–Acceptor Polymers Induced by Asymmetric Structural Isomers for Application to Polymer Solar Cells. ACS Appl Mater Interfaces 2019;11:9239–50. https://doi.org/10.1021/acsami.8b19449.

Conflict of Interest

Declaration of interests

■ The authors declare that they have no known competing financial interests or personal relationships that could have appeared to influence the work reported in this paper.

☐The authors declare the following financial interests/personal relationships which may be considered as potential competing interests: